Research Square

Preprints are preliminary reports that have not undergone peer review.
They should not be considered conclusive, used to inform clinical practice,
or referenced by the media as validated information.

Development of non-contact pH-responsive PAN/Malva sylvestris nanofibrous sensors for intelligent food packaging and meat freshness monitoring

Shabnam Hadadian
Student Research Committee
Ehsan Sadeghi
ehsan.sadeghi59@yahoo.com

Research Center for Environmental Determinants of Health (RCEDH),
Mojtaba Heydari-Majd
Department of Agriculture & Natural Resources

Article

Keywords: Non-contact intelligent packaging, Polyacrylonitrile, Malva sylvestris extract, Electrospinning, Fish freshness indicator

Posted Date: September 23rd, 2026

DOI: https://doi.org/10.21203/rs.3.rs-10745317/v1

License: This work is licensed under a Creative Commons Attribution 4.0 International License.
Read Full License

Additional Declarations: No competing interests reported.

Abstract

This study aimed to develop and characterize a non-contact pH-responsive nanofibrous indicator based on polyacrylonitrile (PAN) and *Malva sylvestris* extract (MFE) for smart food packaging applications. Initially, nanofibers were fabricated using three PAN concentrations (10%, 13%, and 16% w/v), and 13% PAN was selected as the optimal matrix based on morphological and mechanical evaluations. Anthocyanin-rich MFE was then incorporated into the optimized PAN solution at three loadings (10%, 20%, and 30% w/w) to obtain multifunctional colorimetric nanofibers. FTIR and XRD analyses confirmed hydrogen bonding and π–π interactions between PAN nitrile groups and phenolic compounds of MFE, leading to reduced crystallinity and improved molecular cohesion. The PAN/MFE II formulation (20% extract) exhibited the best balance of properties, including high tensile strength (9.36 MPa), thermal stability, and antioxidant activity (47.7% DPPH inhibition). The films showed distinct and reversible color transitions, from pink (pH 2) to purple (pH 7), green (pH 9), and yellow (pH 12), reflecting anthocyanin structural transformations. The nanosensor's practical performance was evaluated in fish (*Otolithes ruber*) packaging under non-contact conditions. During refrigerated storage, color changes of the sensor strongly correlated with increases in fish pH and total volatile basic nitrogen (TVB-N), successfully indicating both early spoilage and full deterioration stages. These findings demonstrate that the PAN/MFE nanofibrous system offers a safe, stable, and sensitive non-contact optical indicator suitable for next-generation intelligent food packaging.

1. Introduction

Maintaining the safety and quality of food products during storage and distribution continues to be a significant challenge faced by the food industry (Heydari-Majd et al., 2019a). Standard expiration dates generally do not provide an accurate indication of the freshness of perishable products in real-time, and therefore will not assist with food safety or consumer satisfaction. In this context, smart packaging technologies that utilize visual sensors to evaluate food quality are gaining interest as an effective method for monitoring food quality. Colorimetric indicators that change color in response to pH changes are an example of a type of indicator that can respond rapidly, are non-destructive, and are easy to use for consumers to interpret food spoilage (Guo et al., 2025).

Colorimetric sensors are commonly made using polymeric matrices that can hold natural pigments in place and withstand structural integrity under wet conditions within food packages. Synthetic polymers such as polyacrylonitrile (PAN) are particularly appealing because of their outstanding mechanical strength, ability to form fibers, and resistance to chemicals. This polymer is distinguished by its low density, high tensile strength, low modulus of elasticity, and limited solubility, attributes that contribute to its cost-effectiveness (Varela et al., 2025). Although PAN is non-biodegradable, it can be safely applied as a non-food-contact indicator label, separated from the food surface, where migration of chemical constituents is negligible. This non-contact approach also aligns with food safety regulations by minimizing any potential contamination risks.

The fabrication of smart packaging materials can involve various techniques, including casting, extrusion, and electrospinning. Electrospinning, in particular, is a process utilized to produce diverse nanofibers and microfibers from polymer solutionsb (Heydari-Majd et al., 2019b). This technique represents one of the most recent advancements in smart film production, noted for its efficiency and cost-effectiveness relative to extrusion methods. Electrospinning generates fibrous materials characterized by a high surface-to-volume ratio and enhanced porosity (Heydari-Majd et al., 2024). The apparatus employed in this process comprises a syringe serving as a polymer reservoir and a metallic needle for fiber extrusion, with fiber formation occurring through three stages: initiation of jet ejection, elongation, and solidification (Waris et al., 2025). Recent developments have seen the application of this technology in producing polymer-based nanofibers for food-related applications. To functionalize PAN nanofiber, additives such as plant extracts and compounds with antimicrobial and antioxidant properties can be incorporated.

Natural plant extracts that contain anthocyanins have garnered significant attention as natural, environmentally-friendly colorimetric agents due to their impressive pH sensitivity and antioxidant properties. The color changes of anthocyanins in *Malva sylvestris L.* (an herbaceous plant of the genus *Malva*) petals transition from pink to green and yellow under differing pH conditions, establishing these petals as new resources for a freshness indicator (Noghani Bahambari et al., 2024). *Malva sylvestris* extract (MFE), a traditional medicinal herb, has been used to alleviate pain and inflammation, promote wound healing, address renal and dermatological conditions, and combat various pathogens including viruses, bacteria, and fungi. Its principal constituents include phenolic and flavonoid compounds, as well as anthocyanins, leuco-anthocyanins, delphinidin, malvidin, beta-carotene, tannins, saponins, alkaloids, and mucilage (Memdueva et al., 2025) The inherent antioxidant capacity of MFE enables it to interact with radicals generated during lipid oxidation, thereby interrupting chain reactions, decelerating oxidative processes, and reducing the rate of spontaneous oxidation. Additionally, MFE is utilized in the manufacture of litmus paper.

Therefore, this study aims to fabricate and characterize pH-responsive electrospun PAN nanofibrous films containing Malva sylvestris extract (MFE) as non-food-contact colorimetric indicators for smart packaging applications. The physicochemical (mechanical, barrier, and moisture-resistance) and optical properties, as well as the antioxidant and color stability of the films, were evaluated to assess their reliability and durability under conditions simulating the internal environment of food packages.

2. Materials and methods

2.1. Reagents

Polyacrylonitrile (PAN, Mw ≈ 150,000) powder and N-dimethylformamide (DMF, analytical grade) were purchased from Sigma-Aldrich (St. Louis, MO, USA). Dried petals of *Malva sylvestris L.* were obtained from a local herbal store a local herbal store (Kermanshah, Iran) and used as a natural source of anthocyanins. The 2,2-diphenyl-1-picrylhydrazyl (DPPH) reagent was acquired from Merck Company

(Weiterstadt, Germany). All other reagents and materials utilized in this study were of analytical grade and high purity.

2.2. *Malva sylvestris extract* (MFE)

The petals were dried at a controlled temperature of 25 ± 1 ºC and ground into fine powder. A 10 g aliquot of this powder was combined with 100 ml of a solvent mixture composed of ethanol and distilled water in a 20:80 v/v ratio. This mixture was continuously stirred using an IKA stirrer (Germany) for 24 h under dark conditions at ambient temperature. The resultant solution was filtered through Whatman No. 4 filter paper and subsequently centrifuged at 6000g for 15 minutes to eliminate residual particulates. The solvent was then concentrated employing a vacuum rotary evaporator at 45°C, following the procedure described by Shavisi & Shahbazi, 2022. The concentrated extract was stored in amber bottles at 4°C until use.

2.3. Fabrication of electrospun PAN/MFE nanofibrous films

Initially, PAN solutions with different concentrations (10, 13, and 16% w/v) were fabricated by dissolving PAN powder in DMF under magnetic stirring at 60°C for 3 h until homogeneous and transparent solutions were obtained. Each solution was electrospun under identical operating conditions to determine the optimal PAN concentration for fiber formation (Almasian et al., 2020). After determining the optimum concentration of PAN for electrospinning, different amount of MFE (10, 20, and 30%, w/w, relative to PAN weight) was added to the polymer solution and it was magnetically stirred at room temperature for 12 h. Electrospinning was carried out using a high-voltage power supply (Fanavaran Nano-Meghyas Co. Iran). The optimized parameters were as follows: applied voltage = 23 kV, tip-to-collector distance = 15 cm, and solution feed rate = 12 mL h^{-1}. The nanofibers were collected on an aluminum foil-covered rotating drum (200 rpm) and then dried in a desiccator at room temperature for 48 h to remove residual solvent (Almasian et al., 2020). After electrospinning, the collected nanofibers were placed in a vacuum desiccator at room temperature for 48 h to ensure complete removal of solvent residues (DMF) and to obtain safe, solvent-free films suitable for food-packaging environments.

The obtained samples were coded as follows: PAN-10, PAN-13, PAN-16 (pure PAN films with different polymer concentrations) and PAN/MFE I, PAN/MFE II, PAN/MFE III (PAN 13% films containing 10, 20, and 30% extract, respectively).

2.4. Intended application and safety consideration

The fabricated nanofibrous films were designed as non-food-contact colorimetric indicator labels intended for use inside food packaging systems but without direct contact with the food surface. In this configuration, the indicator label can be attached to the inner side of the package wall or to the headspace region, allowing it to monitor pH or volatile changes associated with food spoilage while avoiding any material–food interaction. This design concept aligns with current food safety regulations that restrict the use of non-biodegradable synthetic polymers for direct food contact. Therefore, the characterization experiments in this study, including antioxidant activity, moisture resistance, solubility,

and water vapor permeability were conducted to evaluate the stability, durability, and functional reliability of the indicator under humid and oxidative conditions typically present in packaged food environments. These analyses were performed to assess environmental performance rather than to determine the material's suitability for direct food contact.

2.5. Characterization of the nanofibrous films

2.5.1. Scanning electron microscopy (SEM)

The surface morphology and fiber diameter of the electrospun films were examined using a scanning electron microscope (Hitachi S-4800, Japan) at an accelerating voltage of 5.0 kV. Samples were sputter-coated with gold prior to imaging. Fiber diameter distributions were calculated using ImageJ software (National Institutes of Health, USA) from at least 100 random measurements per image. Morphological uniformity and absence of bead formation were considered as criteria for optimal electrospinning conditions (Bahrami et al., 2023).

2.5.2. Thickness

The thickness of the nanofibrous films was measured at three random points using a digital coating thickness gauge (Elcometer A300 FNP 23, Elcometer Instruments Ltd., Manchester, UK) with a precision of 0.001 mm (Heydari-Majd et al., 2022). The average values were used for subsequent calculations of mechanical and water vapor permeability properties.

2.5.3. Moisture content, water solubility, and water vapor permeability (WVP)

The moisture content (MC) was measured gravimetrically by drying films at 105°C until constant weight according to the following formula (1) (Abdolshahi et al., 2022):

$$\text{MC (\%)} = \frac{\mathrm{A}-\mathrm{B}}{\mathrm{A}} \times 100 \quad (1)$$

where, A and B represent the initial and dried sample weights, respectively. The test was replicated three times.

Water solubility (WS) was determined by immersing pre-weighed film pieces in distilled water at 25°C for 24 h and measuring the percentage of dry matter loss after drying using the following Eq. (2) (Niazmand et al., 2025):

$$\text{WS (\%)} = \frac{C-D}{C} \times 100 \quad (2)$$

where C and D are the initial and final dry weights, respectively. Three replicates were analyzed per film formulation.

The water vapor permeability (WVP) of the nanofibrous films was determined according to the procedure described by Heydari-Majd et al., (2022), with slight modifications. Each film sample was carefully sealed to the open mouth of a glass tube containing 10 mL of distilled water, thereby creating a 100% relative humidity (RH) environment inside the tube. The sealed tubes were then placed in a desiccator containing activated silica gel to maintain an external RH of approximately 0%. The total mass of each tube was recorded at 24 h intervals over a period of seven days. The amount of water vapor transmitted through the film was calculated from the linear slope of mass loss versus time, and WVP was computed using Eq. (3):

$$WVP = \frac{\Delta W \times d}{A \times \Delta t \times \Delta p} \times 100 \quad (3)$$

where ΔW is the mass of water lost (g), *d* is film thickness (mm), *A* is the exposed area (m²), Δt is time (h), and Δp is the water vapor pressure difference (Pa).

These analyses were conducted to evaluate the humidity resistance and dimensional stability of the indicator films under conditions typical of sealed food packages rather than for assessing food-contact behavior.

2.5.4. Mechanical properties

Tensile strength (TS) and elongation at break (EAB) were determined using a universal testing machine (WDW-D, Jinan Wenten Test Instrument Co., Ltd., Jinan, China). Film strips (10 × 50 mm) were conditioned at 25°C and 50% RH for 48 h prior to testing at a crosshead speed of 10 mm min^{-1} (Salarbashi et al., 2020). These parameters were evaluated to ensure that the nanofibrous indicators possess sufficient mechanical stability for handling and placement within packaging systems.

2.6. Structural properties of nanofibrous films

2.6.1. Fourier transform infrared (FTIR) spectroscopy

Fourier-transform infrared (FTIR) spectroscopy analysis of the nanofiber samples was performed utilizing the IRT-Racer 100 spectrometer (Shimadzu, Japan) in conjunction with the potassium bromide (KBr) pellet technique. Spectral data were acquired at a resolution of 4 cm^{-1}, with each sample subjected to 32 scans over a wavenumber range spanning from 4000 to 400 cm^{-1} (Hoseinpour et al., 2025b)

2.6.2. The X-ray diffraction (XRD)

The crystalline structure of the nanofibers was analyzed by X-ray diffraction (Philips PW1830, The Netherlands) using Cu Kα radiation (λ = 0.154 nm) at 40 kV and 30 mA. Data acquisition was performed over a scattering angle range of 2θ = 1° to 100°, employing a scanning rate of 0.02° per minute, in accordance with the specifications outlined in BS EN 13925–1 (2003) (Hoseinpour et al., 2025a).

2.6.3. Differential scanning calorimetry (DSC)

Thermal transitions and stability were evaluated using a DSC 1 Mettler Toledo analyzer. Samples (5–10 mg) were heated from 25 to 300°C at a rate of 10°C min^{-1} under nitrogen atmosphere (20 mL min^{-1}). Changes in glass transition (T_g) and melting temperature (T_m) were used to assess the influence of extract incorporation on thermal behavior (Heydari-Majd et al., 2023).

2.7. Color parameters

The color characteristics of the nanofibrous films were measured using a colorimeter (SC-80C, Shenzhen 3NH Technology, China). The parameters *L** (lightness), *a** (red–green), and *b** (yellow–blue) were recorded to describe the chromatic properties of the films. The total color difference (ΔE) between samples was calculated according to Eq. (4) (Bahrami et al., 2022):

$$\Delta E = \sqrt{(L_0^* - L^*)^2 + (a_0^* - a^*)^2 + (b_0^* - b^*)^2} \quad (4)$$

where L^*, a^* and b^* are the color parameters of each sample at a given pH value, and L_0^*, a_0^* and b_0^* correspond to the color of the reference film at neutral pH (7.0). These measurements were conducted to evaluate the visual response accuracy and reproducibility of the indicator films under varying pH conditions.

2.7.1. Color responses of MFE

The pH-dependent color response of the *Malva sylvestris* extract was examined following the method of Salarbashi et al. (2020). Briefly, 1 mL of MFE was mixed with 30 mL of buffer solutions with pH values ranging from 2 to 12. The mixtures were allowed to equilibrate for 10 min at ambient temperature, and the resulting color changes were visually documented using a digital camera. This preliminary test verified the intrinsic pH sensitivity of MFE, which provides the functional basis for its incorporation into nanofibrous indicator films.

2.8. pH-sensitivity of nanofibrous films in different buffer solutions

The colorimetric response of the PAN/MFE nanofibrous films to different pH environments was determined according to the method of Salarbashi et al. (2020), with slight modifications. Square film samples (3 × 3 cm) were placed in buffer solutions (pH 2–12) for 5 min at room temperature, removed, and dried at ambient conditions. Digital photographs of the films were taken immediately after exposure to capture visual color transitions. The *L**, a*, and *b** color values of each film were then quantified using a Hunter Lab colorimeter (Minolta CR-400, Japan), and the total color difference (ΔE) was calculated using Eq. (4).

The pH-sensitivity evaluation was conducted to determine the ability of the developed non-contact indicator films to visually signal changes in environmental pH, simulating the chemical variations occurring in food packages during storage.

2.9. Application of nanosensor as a non-contact fish freshness indicator

Fish samples (Otolithes ruber) were purchased from a certified local fish market in Kermanshah, Iran, and immediately transported to the laboratory under chilled conditions (4°C). The study was conducted on post-mortem commercial fish samples, and no live animals were used. Therefore, ethical approval was not required. All procedures complied with relevant institutional and national regulations. The practical performance of the developed PAN/MFE nanosensor as a non-contact freshness indicator was evaluated using Tiger Tooth Croaker *(Otolithes ruber)* fillets. Approximately 100 g of fish was placed in airtight polypropylene containers, and a 3 × 3 cm PAN/MFE II nanosensor label was affixed to the inner side of each lid with double-sided adhesive, avoiding any direct contact with the sample. This setup enabled interaction only with volatile compounds generated in the headspace during storage. Samples were stored at 4°C, and at predetermined intervals (0, 4, 8, 12 and 16 days), the color change of the nanosensor was visually recorded. Simultaneously, fish pH and TVB-N values were measured as reference indicators to correlate with the sensor's response. No migration or condensation was observed on the indicator surface during storage, confirming the stability of the non-contact setup.

2.9.1. TVB-N and pH measurement in fish fillets

The total volatile basic nitrogen (TVB-N) content of fish samples was analyzed according to the steam distillation method described by Aghaei et al., (2018). Briefly, 10 g of homogenized fish flesh was mixed with 2 g of magnesium oxide, 300 mL of distilled water, and a few boiling chips, then heated to boiling for 15 min. The released volatile bases were collected in 25 mL of 2% boric acid containing methyl red indicator. After 25 min of steam distillation, the distillate was titrated with 0.1 N H_2SO_4 until the color changed from green to pink. The TVB-N value (mg N/100 g sample) was obtained by multiplying the acid volume (mL) consumed in titration by Aghaei et al., (2018) the factor 14.

The pH of the fish samples was determined following the method described by with minor adjustments. Approximately 10 g of minced fish muscle was blended thoroughly with 100 mL of deionized water to obtain a uniform suspension. The pH value of the resulting homogenate was then measured using a calibrated digital pH meter (Model 780, Metrohm, Switzerland) at room temperature.

2.10. Statistical analysis

All data are expressed as the mean ± standard deviation (SD) derived from three replicates for each experimental condition. Statistical significance among the results was assessed using Duncan's multiple range test at a significance level of $p < 0.05$. All analyses were performed utilizing SPSS software, version 26.0 (IBM Corp., USA).

.

3. Results and discussion

3.1. Scanning electron microscopy (SEM)

The morphological characteristics of electrospun nanofibers depend on several processing variables during electrospinning, including polymer concentration, the distance between the needle tip and collector, solution flow rate, and applied direct current voltage. Among these factors, polymer concentration plays a particularly crucial role in controlling fiber morphology (Miri et al., 2016). The structural characteristics of electrospun fibers directly influence their mechanical properties, specific surface area, and optical characteristics, parameters that are essential for the functionality of headspace-deployed, non-contact colorimetric sensing systems. Figure 1 presents representative SEM images illustrating pure PAN fibers prepared at varying concentrations (10, 13, and 16% w/v) alongside PAN/MFE composite structures containing different mass fractions of MFE (10, 20, and 30%).

Electrospinning of PAN solutions at concentrations of 10% and 16% resulted in fiber structures exhibiting noticeable bead-like defects and nodular irregularities (Fig. 1a, 1c), which suggest unstable jet behavior and suboptimal spinning conditions. Conversely, the 13% PAN solution (Fig. 1b) generated uniform, bead-free fibers with consistent morphological features; consequently, this concentration was adopted for all subsequent composite preparations. These observations align well with established electrospinning principles, which indicate that insufficient polymer concentration leading to reduced solution viscosity, facilitates bead formation, whereas excessively elevated concentrations can induce jet instabilities and morphological imperfections (Heydari-Majd et al., 2019[b]).

The addition of MFE substantially altered the resulting fiber morphology. Fibers containing 10% MFE maintained relatively uniform structures, though minor surface irregularities were evident (PAN/MFE I, Fig. 1d). When the extract concentration was increased to 20% (PAN/MFE II, Fig. 1e), the fibers exhibited optimal characteristics, displaying smooth surfaces, homogeneous structure, and a narrow size distribution; this formulation was thus selected as the most suitable composition. The enhanced morphological quality observed at this intermediate loading level can be attributed to favorable modifications in solution rheology, including viscosity, electrical conductivity, and interfacial tension that promote jet stability during electrospinning and facilitate uniform fiber elongation (Mushtaq et al., 2022). However, at the maximum loading level (30% MFE, PAN/MFE III, Fig. 1f), localized particle agglomeration and increased surface roughness became apparent, suggesting phase incompatibility or accelerated solvent evaporation leading to the deposition of incompletely dissolved extract particles onto the fiber surface (Zhang et al., 2016). Similar morphological phenomena have been documented by Zhang et al., (2017), who observed the formation of interconnected polylactic acid (PLA) network structures upon incorporating 15% Tea Tree and Manuka essential oils into polymer solutions. The morphological alterations characterized by fiber coalescence were attributed to moisture uptake and thermal property mismatches between the polymer matrix and the essential oil components.

From an application perspective, the observed morphology of PAN/MFE II (uniform, bead-free, and smooth fibers) is advantageous for a non-contact indicator: the high surface area and homogeneous

distribution of pigment favor rapid and reproducible interaction with headspace vapors and more consistent colorimetric response.

Insert Fig. 1, about here

3.2. Thickness of nanofibrous

The mean film thickness values measured at three random positions are presented in Table 1. Pure PAN films exhibited the highest average thickness (90.4 ± 11 μm). Incorporation of MFE markedly reduced the thickness: PAN/MFE I = 35.03 ± 1.25 μm, PAN/MFE II = 39.53 ± 1.12 μm, and PAN/MFE III = 30.26 ± 1.56 μm. Different lowercase letters in Table 1 indicate statistically significant differences among treatments ($p < 0.05$). The average thickness values were used in subsequent calculations of tensile properties and WVP.

Table 1
Properties of PAN/MFE film prepared by electrospinning.

Nanofibers	**Thickness (μm)**	**TS (MPa)**	**E (%)**	**WVP ($\times 10^{-11}$ gm^{-1}s^{-1}Pa^{-1})**	**WS (%)**	**MC (%)**
PAN	90.4 ± 11^{a}	6.16 ± 0.05^{d}	65.44 ± 4.41^{a}	5.58 ± 0.04^{a}	17.08 ± 0.13^{a}	37.04 ± 0.21^{a}
PAN/MFE I	35.03 ± 1.25^{c}	7.5 ± 0.18^{b}	24.4 ± 2.04^{d}	5.3 ± 0.02^{b}	16.16 ± 0.3^{b}	26.11 ± 0.15^{b}
PAN/MFE II	39.53 ± 1.12^{b}	9.36 ± 0.93^{a}	35.32 ± 4.16^{b}	3.66 ± 0.12^{d}	15.06 ± 0.1^{c}	15.26 ± 0.39^{d}
PAN/MFE III	30.26 ± 1.56^{d}	6.68 ± 0.05^{c}	29.53 ± 2.55^{bc}	4.65 ± 0.21^{c}	15.66 ± 0.22^{c}	19.95 ± 0.62^{c}

a-d Different lowercase letters in the same column indicate significant differences *($P < 0.05$)*. Data are shown as mean ± standard deviation (n = 3).

The substantial decrease in film thickness observed upon MFE addition, compared to pure PAN, can be explained by extract-induced modifications in solution rheology and electrospinning dynamics. The presence of hydrophilic bioactive compounds typically modifies key solution parameters, including viscosity, electrical conductivity, and interfacial tension. These alterations frequently facilitate the generation of finer fiber diameters and more compact fiber arrangement on the collector surface, consequently leading to reduced mat thickness. The moderately elevated thickness observed for PAN/MFE II relative to PAN/MFE I and III suggests that the 20% extract concentration achieves an optimal rheological balance, producing uniform fibers with marginally increased diameters or enhanced layer deposition. In contrast, the highest extract loading (PAN/MFE III) appears to promote particle agglomeration and phase incompatibility, (as evidenced by SEM analysis), potentially generating thinner yet more heterogeneous fiber deposition, which accounts for the minimum thickness value recorded.

From a functional perspective, film thickness directly influences mechanical behavior and barrier performance: thinner mats normally exhibit lower elongation and can show reduced WVP because of tighter fiber packing, but extreme thinning or irregular structure (as in PAN/MFE III) can increase defect density and reduce mechanical robustness. The measured thickness trends therefore help explain the observed increase in tensile strength for PAN/MFE II and the lower elongation values across composite films (Table 1).

Insert Table 1, about here

3.3. Moisture content, water solubility, and water vapor permeability (WVP)

The results for MC, WS, and WVP of the PAN and PAN/MFE nanofibrous films are summarized in Table 1. The MC of pure PAN film was relatively low (3.74 ± 0.11%), reflecting the hydrophobic nature of the polymer matrix. Incorporation of MFE significantly reduced MC ($p < 0.05$). Also, WS decreased slightly with extract addition.

Although anthocyanins are inherently hydrophilic due to the presence of multiple hydroxyl and methoxy groups, their incorporation into the PAN matrix can paradoxically enhance the apparent hydrophobicity of the resulting composite films. This effect originates from both molecular interactions and morphological modifications induced by the extract. At the molecular level, the polar hydroxyl groups of anthocyanins can form hydrogen bonds or dipole–dipole interactions with the nitrile (–C ≡ N) groups of PAN. Such interactions effectively “shield” some of the hydrophilic sites of both components from direct exposure to water molecules, thereby reducing overall water uptake and leading to lower MC in the composite films. Additionally, π–π stacking between aromatic rings of anthocyanins and PAN chains may contribute to a more compact molecular packing, limiting the penetration of water into the polymer matrix.

Morphologically, the incorporation of MFE resulted in a noticeable decrease in fiber diameter and a denser nanofiber network, as observed in SEM images. The finer and more tightly packed fibers reduce the number of capillary voids available for moisture retention, further contributing to the observed decrease in MC. These effects collectively explain the pronounced reduction in moisture content in PAN/MFE composites compared to pure PAN.

Moreover, the intrinsic hydrophobicity of PAN itself provides resistance to water absorption and swelling. When combined with plant-derived pigments and phenolic compounds, the film’s surface chemistry is modified in a way that enhances interactions between the less polar constituents of the extract and the PAN backbone. This synergistic effect increases the overall hydrophobicity and reduces WS. Similar enhancements in water resistance following incorporation of natural pigments have been reported by Shakouri et al. (2023) and Yavari Maroufi et al. (2022), who attributed these changes to improved polymer–filler compatibility and reduced surface polarity.

Consistent findings have also been documented by Huang et al. (2020), who observed decreased surface wettability in polyvinyl alcohol films containing sour tea anthocyanins, and by Zhai et al., (2017), who reported reduced MC in starch/PVA films after anthocyanin incorporation. Together, these results confirm that the addition of MFE to PAN nanofibers modifies both the chemical and physical structure of the film, improving its resistance to humidity and lowering solubility, essential features for stable, non-contact colorimetric indicators operating in humid packaging environments.

WVP is a critical parameter in food packaging applications, as the packaging film must effectively inhibit moisture transfer from the external environment to the interior of the package. WVP values ($\times 10^{-11}$ g m^{-1} s^{-1} Pa^{-1}) followed a non-linear trend: PAN = 5.58 ± 0.04, PAN/MFE I = 5.30 ± 0.02, PAN/MFE II = 3.66 ± 0.12 (lowest), and PAN/MFE III = 4.65 ± 0.21; differences among treatments were statistically significant ($p < 0.05$) (Table 1). The observed reduction in WVP for PAN/MFE composites, particularly at 20% extract loading, can be attributed to both morphological and molecular factors. The incorporation of MFE led to smaller fiber diameters and a denser nanofiber network, increasing tortuosity and reducing vapor diffusion pathways (Huang et al., 2019). Moreover, hydrogen bonding and π–π interactions between anthocyanins and PAN chains limited the accessibility of polar groups, thereby reducing water adsorption and permeability (Ardjoum et al., 2023). At higher extract concentrations (30%), phase separation and fiber irregularities generated microvoids, which increased WVP again. This non-linear behavior aligns with previous findings on anthocyanin- and extract-based electrospun films (Zhai et al., 2017; Mushtaq et al., 2018; Chen et al., 2023). Overall, the optimized PAN/MFE II formulation achieved the best barrier efficiency and humidity stability, essential for non-contact headspace indicator applications.

3.4. Mechanical properties

The mechanical performance of the nanofibrous films was evaluated through tensile strength (TS) and elongation at break (E), which reflect the film's resistance to stress and flexibility during handling and storage (Mushtaq et al., 2018). As shown in Table 1, pure PAN exhibited a TS of 6.16 MPa, while incorporation of MFE significantly improved TS, reaching 9.36 MPa in PAN/MFE II. This enhancement is attributed to hydrogen bonding and secondary interactions between anthocyanin functional groups and the nitrile groups of PAN, which reinforce chain packing and stress transfer (Kossyvaki et al., 2022).

At higher extract loading (30%), phase separation and aggregation occurred, weakening inter-fiber cohesion and reducing TS (Safaee-Ardakani et al., 2019; Heydari-Majd et al., 2022). Conversely, E decreased from 65.44% (PAN) to 35.32% (PAN/MFE II), indicating that the presence of MFE restricted polymer chain mobility and increased stiffness within the matrix. The inverse relationship between TS and E, higher strength but lower flexibility, suggests that moderate extract loading optimizes interfacial bonding without causing brittleness. Such characteristics are desirable for non-contact colorimetric films, where mechanical stability is prioritized over extensibility.

3.5. Fourier transform infrared (FTIR) analysis

Figure 2, displays the FTIR spectra of PAN, PAN/MFE I, PAN/MFE II, and PAN/MFE III nanofiber indicators. For pure PAN, the characteristic absorption bands appeared at 2940 cm^{-1}, 2244 cm^{-1}, 1726 cm^{-1}, 1629 cm^{-1}, 1445 cm^{-1}, and 1260 cm^{-1}, corresponding to C–H stretching, C ≡ N stretching, C = O stretching, C = C vibrations of the pyrrole ring, and C–N stretching within the polymer backbone.

After incorporating MFE, notable spectral changes were observed. The C = O stretching peak around 1039 cm^{-1} and the N–H hydrogen-bond stretching band near 1746 cm^{-1} both shifted toward lower wavenumbers and decreased in intensity, particularly in the PAN/MFE II sample. These shifts indicate the formation of new hydrogen bonds between hydroxyl or carbonyl groups of anthocyanins and the nitrile groups of PAN, leading to improved molecular compatibility and structural compactness. Such hydrogen-bond interactions can increase film strength and reduce hydrophilicity, consistent with the enhanced mechanical performance of PAN/MFE II (Nunes et al., 2021).

At higher extract loading (PAN/MFE III), the progressive reduction in peak intensity suggests weaker molecular interactions and possible phase separation due to excess phenolic compounds (Liu et al., 2019). Similar spectral shifts associated with hydrogen bonding between polymer matrices and plant extracts have been reported in sodium alginate/nano-silica/oregano extract films (Lu et al., 2021) and in pectin/blackberry extract systems (Shivangi et al., 2021). Overall, the FTIR spectra confirm that moderate extract incorporation (20% MFE) promotes effective molecular bonding between PAN and MFE, thereby enhancing nanofiber structural integrity (Moradi et al., 2019).

Insert Fig. 2, about here

3.6. The X-ray diffraction (XRD)

Figure 3 shows the X-ray diffraction (XRD) profiles of pure PAN and PAN/MFE nanofibers. The pristine PAN exhibited a sharp diffraction peak around 2θ = 17°, characteristic of its semi-crystalline structure (Zhang et al., 2019). Upon incorporation of MFE, the diffraction peaks became broader and less intense within the 17°–28° 2θ region, indicating a reduction in crystallinity. This decrease may be attributed to the formation of new hydrogen bonds between PAN chains and polar components of MFE, which disturb molecular packing and hinder the growth of crystalline domains (Sun et al., 2019). A decline in peak intensity may also arise from partial retention of solvent (DMF) and from the structural rearrangement induced during electrospinning. Rapid jet stretching and solvent evaporation can restrict time for ordered chain alignment, leading to an amorphous morphology (Karbownik et al., 2019; Córdoba & Sobral, 2017). Finally, partial solvent retention or non-uniform extract dispersion may attenuate diffraction intensity, further lowering the apparent crystallinity.

Similarly, Wang et al. (2007) observed that adding black-soybean-husk extract to chitosan/gelatin films disrupted regular molecular organization, supporting the idea that phenolic compounds can interfere with polymer chain ordering. Overall, the broader peaks and decreased intensity in the PAN/MFE diffractograms confirm that extract incorporation decreases the crystallinity of PAN nanofibers, consistent with the improved flexibility and reduced stiffness observed in mechanical tests.

Insert Fig. 3, about here

3.7. Differential scanning calorimetry (DSC)

Figure 4 shows the thermal behavior of pure PAN and PAN/MFE nanofibers as obtained from differential scanning calorimetry (DSC). All nanofibers exhibited two major stages of thermal transition. The first weight-loss stage (35–45°C) corresponds to the evaporation of residual moisture and volatile compounds entrapped within the nanofiber matrix (Tretsiakova-McNally & Joseph, 2018). The second degradation stage (290–300°C) is attributed to the main-chain decomposition of PAN, involving cyclization and oxidation reactions of nitrile groups, as well as intermolecular and intramolecular crosslinking processes that occur during the stabilization phase of PAN (Wang et al., 2007).

A noticeable decrease in melting temperature (Tm) was observed for the PAN/MFE I sample, suggesting reduced crystallinity and a more disordered molecular arrangement caused by hydrogen bonding between anthocyanin phenolics and the PAN matrix. Conversely, the PAN/MFE II sample showed an increase in T_m, indicating stronger polymer–extract interactions, denser chain packing, and lower free-volume mobility due to partial dehydration and improved matrix cohesion. These findings are in agreement with the XRD results showing reduced crystallinity but enhanced structural compactness.

In addition, incorporation of MFE shifted the T_g to higher values, confirming the establishment of hydrogen bonds between the phenolic hydroxyls of MFE and nitrile groups of PAN, which restrict polymer chain motion and improve thermal resistance. A similar enhancement in thermal stability was reported by Huang et al. (2020), who found that incorporation of Roselle anthocyanins into hydroxypropyl methylcellulose–polyvinyl alcohol films increased Tg and delayed the onset of degradation due to strong polymer–phenolic interactions. Overall, the DSC results demonstrate that moderate extract incorporation (20% MFE) effectively enhances the thermal stability of PAN nanofibers by promoting interfacial bonding and reducing chain mobility.

Insert Fig. 4, about here

3.8. Color parameters

Table 2 summarizes the colorimetric parameters (L^*, a^*, b^*, and ΔE) for PAN and PAN/MFE nanofibers. Incorporation of MFE produced pronounced color variations compared with pure PAN. As the extract concentration increased from 10% to 30% (w/v), the L^* (lightness) and b^* (yellow-blue) values significantly increased ($p < 0.05$), while the total color difference (ΔE) also rose, indicating an overall shift toward brighter and more bluish-green hues. This color modification arises from the anthocyanins present in MFE, which exhibit pH- and polarity-dependent color transitions (He et al., 2022).

Table 2
Color parameters including *L**, *a**, *b** and Δ*E* of PAN and PAN/MFE nanofibers.

nanofibers	L*	a*	b*	ΔE
PAN	98.21 ± 0.11^{d}	3.87 ± 0.78^{c}-	11.55 ± 0.01^{c}	7.13 ± 0.49^{d}
PAN/MFE I	108.96 ± 0.85^{b}	-5.81 ± 0.41^{bc}	12.61 ± 0.03^{b}	13.35 ± 0.7^{c}
PAN/MFE II	128.35 ± 24.04^{a}	-8.89 ± 0.17^{a}	13.79 ± 0.98^{a}	26.29 ± 0.39^{a}
PAN/MFE III	112.51 ± 0.48^{c}	-7.26 ± 0.19^{b}	13.99 ± 2.42^{a}	19.93 ± 0.33^{b}

Values are given as mean ± SD (n = 3). Different lowercase letters in the same column indicate significantly different ($p < 0.05$).

The observed increase in *L** can also be linked to reduced nanofiber diameter, as evidenced by SEM images. Finer fibers enhance light scattering and reflection while diminishing absorption, leading to greater brightness and higher *L** values (He et al., 2022). Similarly, the presence of uniformly dispersed anthocyanins within the PAN matrix promotes a more homogeneous optical surface, amplifying overall color intensity and chromatic stability.

The characteristic blue-violet tone of PAN/MFE fibers results from anthocyanin–polymer interactions that stabilize the quinonoidal base form of anthocyanins under the slightly neutral environment of PAN (Prietto et al., 2018). As extract loading increased, stronger π–π stacking and hydrogen bonding between PAN nitrile groups and anthocyanin aromatic rings enhanced pigment retention and shifted chromatic balance toward blue regions.

Comparable effects have been reported for biopolymer matrices containing anthocyanins. For instance, Kurek et al. (2018) demonstrated that chitosan films with blueberry extract exhibited higher *L**, *a**, and *b** values, while Prietto et al. (2018) observed that raising red cabbage anthocyanin content in zein nanofibers from 3% to 5% significantly increased ΔE, confirming concentration-dependent chromatic enhancement. Overall, the increasing ΔE and *L** values of PAN/MFE composites confirm the effective incorporation and optical activation of anthocyanins, which impart distinct visual contrast desirable for intelligent non-contact labels in food-quality monitoring systems.

Insert Table 2, about here

3.9. Color changes of the MFE

The predominant anthocyanins in MFE are acylated derivatives of malvidin and delphinidin, with a total anthocyanin concentration of approximately 1.8 mg/100 mL at pH 5.4. As shown in Fig. 5a, the extract exhibited distinct color transitions and corresponding UV–Vis spectral variations across the pH range 2–12. At acidic pH 2, the extract appeared pink with a strong absorption band near 525 nm, corresponding to the flavylium cation form. As pH increased toward neutrality, this band gradually decreased and vanished around pH 7, indicating structural conversion to carbinol and quinoidal bases. At pH 8–9, the

solution turned bluish-green, accompanied by a new absorption peak shift toward 520 nm, and under strongly alkaline conditions (pH > 9), a grey–green color emerged, consistent with the formation of ionized anhydrobase species (Alizadeh-Sani et al., 2021).

These pH-dependent chromatic transitions are attributed to reversible structural transformations among multiple anthocyanin forms, including the red flavylium cation (pH < 3), colorless carbinol pseudobase (pH 4–5), purple-blue quinoidal base (pH 6–8), and greenish ionized anhydrobase (pH > 9) (Dangles & Fenger, 2018). The variation in hue intensity and stability arises from the degree of hydroxylation and methoxylation on the anthocyanidin B-ring: malvidin, possessing two methoxy (-OCH_3) groups, contributes to purple coloration and higher pigment stability, whereas delphinidin, containing hydroxyl (–OH) groups, shifts the hue toward blue tones (Habtemariam, 2019). Both substituents act as electron-donating groups, enhancing π-electron delocalization and thus increasing molecular resonance stability and chromatic intensity (Seddighfar et al., 2020).

Similar behavior has been observed in other natural extracts, such as purple-fleshed sweet potato anthocyanins, where progressive color changes from red to blue are associated with transformations between flavylium and quinoidal forms (Kang et al., 2020; Yong et al., 2019).

Collectively, these findings confirm that the wide color range of MFE results from the coexistence of multiple anthocyanidin structures and their reversible acid–base interconversion. This underpins the excellent pH-responsiveness and optical versatility of the extract for non-contact intelligent indicator applications.

Insert Fig. 5, about here

3.10. Color change of PAN/MFE

As shown in Fig. 5b, the PAN/MFE nanofiber indicator exhibited distinct and reversible color transitions across the tested pH range. The color shifted from pink at pH 2, to purple around pH 6–7, green at pH 8–9, and finally yellow at pH 12, mirroring the pH-dependent structural conversions of anthocyanins in the embedded MFE extract. The gradual fading of pink coloration up to pH 6 reflects the transformation of flavylium cations into less conjugated carbinol and quinoidal species (Alizadeh-Sani et al., 2021).

A key observation is that the PAN/MFE indicator retained visible chromatic sensitivity in the near-neutral range (pH 5–7), which is critical for monitoring food freshness, as many spoilage reactions and pH drifts occur within this interval. This property distinguishes the indicator from conventional systems that typically respond only under strongly acidic or alkaline conditions (Ghorbani et al., 2021).

From a physicochemical perspective, the immobilization of anthocyanins within the semi-hydrophobic PAN matrix creates a microenvironment that moderates proton exchange and stabilizes intermediate chromophores. This confinement effect allows the pigment to exhibit controlled, gradual color transitions even without direct contact with aqueous media, making it ideal for non-contact intelligent labeling applications. Additionally, interactions between anthocyanin hydroxyl groups and PAN nitrile

moieties (via hydrogen bonding and π–π stacking) further restrict molecular degradation, maintaining color intensity during pH exposure cycles (Dangles & Fenger, 2018).

Comparable findings have been reported for anthocyanin-based colorimetric indicators incorporated into polymeric matrices, where pigment–polymer interactions stabilize intermediate forms and enable consistent responses over repeated pH fluctuations (Alizadeh-Sani et al., 2021; Ghorbani et al., 2021). Collectively, these results confirm that the PAN/MFE nanofiber indicator offers reliable, reversible, and visually discernible color transitions suitable for non-contact monitoring of food freshness in mildly acidic to neutral environments.

3.11. Chemical changes in fish

A low concentration of TVB-N reflects limited microbial activity and minimal spoilage in seafood. As microorganisms proliferate and metabolize proteins, they release nitrogenous bases such as ammonia and various amines (primary, secondary, and tertiary). The initial TVB-N content of the fish samples was approximately 14.12 mg N/100 g (Fig. 6a), which is comparable to the 13.43 mg N/100 g reported by (Heydari-Majd et al., 2019a) for *O. ruber* fillets. Over time, the TVB-N level increased steadily with storage. According to the European Commission (CEC, 1995), the maximum acceptable TVB-N concentration for seafood is 35 mg N/100 g. After 12 days of storage, the TVB-N value reached 34.2 mg N/100 g, still within the legal limit, though the fish began to exhibit noticeable changes in appearance, such as excessive surface moisture. This stage may therefore serve as a visual warning for both consumers and retailers. By day 16, TVB-N had increased to 43.4 mg N/100 g, surpassing the acceptability threshold; the fillets became soft, watery, and emitted an unpleasant odor, indicating clear spoilage. Previous research by Balamatsia et al., (2007) and Aghaei et al., (2018) has confirmed that TVB-N and related biogenic amines can serve as reliable chemical indicators for assessing microbial quality in perishable products such as fresh poultry and seafood.

The initial pH of the fish fillets was 6.20 and gradually increased during storage, reaching 7.2 by day 16 (Fig. 6b). This rise is mainly attributed to microbial metabolism and enzymatic degradation of proteins, leading to the release of alkaline compounds such as ammonia and trimethylamine (Heydari-Majd et al., 2019a). The accumulation of these volatile nitrogenous bases causes tissue breakdown and a decline in overall meat quality. Similar pH trends during storage have been observed in various fish species. (Kyrana et al., 1997) reported no major pH variation in *Sparus aurata* during the early storage period, followed by a noticeable increase after the seventh day. Later, Kyrana and Lougovois, (2002) linked sharp pH rises beyond the 12th day to accelerated spoilage. Since pH thresholds differ depending on factors such as species, catch season, and handling (Pacquit et al., 2006), no universal limit can be defined. Based on the combined results of pH and TVB-N analyses, the estimated shelf life of fish stored at 4°C was about 12 days, aligning with the findings of Heydari-Majd et al., (2019a), who reported 12 days for *O. ruber* fillets under similar conditions.

Insert Fig. 6, about here

3.11.1. Colorimetric analysis

The PAN/MFE nano sensor initially appeared white. As the concentration of TVB-N increased during storage, the headspace pH also rose, triggering visible color transitions in the nanosensor. No noticeable color change occurred within the first 72 h at 4°C, but after the fourth day, a lemon-yellow color appeared by the eighth day and gradually becoming lighter on day 12 and finally exhibiting a yellowish-green hue on day 16 (Fig. 7). Accordingly, the pale-yellow appearance on day 12 represented the consumer warning stage, whereas the yellowish-green coloration detected on day 16 signified complete spoilage. This pattern indicates that the developed indicator can signal both the early warning stage and the final spoilage point of fish. The chemical analysis results confirmed this behavior. Similarly, (Silva-Pereira et al., 2015) observed delayed color transitions under refrigerated conditions, where the indicator shifted from blue to yellow after seven days, coinciding with spoilage-related pH increases.

Insert Fig. 7, about here

4. Conclusion

This research successfully developed a non-contact pH-responsive colorimetric nanosensor composed of polyacrylonitrile (PAN) and *Malva sylvestris* extract (MFE) for intelligent food packaging applications. The vacuum-dried PAN/MFE nanofibers exhibited no detectable odor or residual solvent traces, confirming complete removal of DMF and ensuring non-toxicity for non-contact applications. The vacuum-dried PAN/MFE nanofibers exhibited no detectable odor or residual solvent traces, confirming complete removal of DMF and ensuring non-toxicity for non-contact applications. The systematic optimization of PAN concentrations (10%, 13%, and 16%) and extract loadings (10%, 20%, and 30%) led to the identification of an optimal formulation (PAN/MFE II, 13% PAN with 20% MFE) exhibiting uniform morphology, high mechanical strength, and excellent stability. Spectroscopic analyses confirmed strong intermolecular interactions between PAN and MFE, contributing to improved cohesion and reduced crystallinity. The nanofibers demonstrated distinct and reversible color transitions over a wide pH range, validating their suitability as optical indicators. When tested as a non-contact freshness sensor for fish (*Otolithes ruber*), the developed films accurately tracked quality changes through headspace volatiles, with color shifts correlating well with pH and TVB-N values during refrigerated storage. The results confirm that the PAN/MFE nanosensor provides a safe, stable, and effective tool for visual monitoring of food freshness without direct food contact. Overall, this system represents a promising step toward next-generation intelligent packaging technologies that integrate visual, non-invasive freshness indicators for improved food safety and consumer confidence. Future studies should focus on integrating the PAN/MFE indicator into biodegradable multilayer systems for industrial scalability.

Declarations

Acknowledgement

The authors acknowledge the technical support provided by the laboratory staff of Kermanshah University of Medical Sciences during the course of this research.

Conflicts of Interest

The authors declare no conflict of interest

Funding statement

This research was approved and supported by the Student Research Committee, Kermanshah University of Medical Sciences, Kermanshah, Iran (Grant Number: 4010687). The funding body had no role in the study design, data collection, analysis, interpretation, or manuscript preparation.

Author contributions (CRediT taxonomy)

All authors meet the criteria for authorship as outlined by the International Committee of Medical Journal Editors (ICMJE). Specifically:

Shabnam Hadadian: Writing – original draft, Methodology, Investigation, Formal analysis, Visualization. **Ehsan Sadeghi:** Conceptualization, Supervision, Project administration, Funding acquisition, Validation, Writing – review & editing. **Mojtaba Heydari-Majd:** Conceptualization, Supervision, Resources, Software, Methodology, Validation, Writing – review & editing.

All authors reviewed and approved the final version of the manuscript. They agree to be accountable for all aspects of the work, ensuring that questions related to the accuracy or integrity of any part of the work are appropriately investigated and resolved.

References

1. ABDOLSHAHI, A., MAJD, M. H., ABDOLLAHI, M., FATEMIZADEH, S. & MARVDASHTI, L. M. 2022. Edible Film Based on Lallemantia peltata L. Seed Gum: Development and Characterization. *Journal of Chemical Health Risks*, 12.
2. AGHAEI, Z., EMADZADEH, B., GHORANI, B. & KADKHODAEE, R. 2018. Cellulose acetate nanofibres containing alizarin as a halochromic sensor for the qualitative assessment of rainbow trout fish spoilage. *Food and bioprocess technology*, 11, 1087–1095.
3. Alizadeh-Sani, M., Tavassoli, M., McClements, D. J., & Hamishehkar, H. (2021). Multifunctional halochromic packaging materials: Saffron petal anthocyanin loaded-chitosan nanofiber/methyl cellulose matrices. *Food hydrocolloids*, *111*, 106237.
4. Almasian, A., Najafi, F., Eftekhari, M., Ardekani, M. R. S., Sharifzadeh, M., & Khanavi, M. (2020). Polyurethane/carboxymethylcellulose nanofibers containing Malva sylvestris extract for healing diabetic wounds: Preparation, characterization, in vitro and in vivo studies. *Materials Science and Engineering: C*, *114*, 111039.
5. Ardjoum, N., Chibani, N., Shankar, S., Salmieri, S., Djidjelli, H., & Lacroix, M. (2023). Incorporation of Thymus vulgaris essential oil and ethanolic extract of propolis improved the antibacterial, barrier

and mechanical properties of corn starch-based films. *International Journal of Biological Macromolecules*, *224*, 578–583.

6. Aslam, M., Khan, T., Basit, M., Masood, R., & Raza, Z. (2022). Polyacrylonitrile-based electrospun nanofibers–A critical review. *Materialwissenschaft und Werkstofftechnik*, *53*(12), 1575–1591.
7. Athauda, T., Banerjee, P. C., & Karmakar, N. C. (2020). Microwave characterization of chitosan hydrogel and its use as a wireless pH sensor in smart packaging applications. *IEEE Sensors Journal*, *20*(16), 8990–8996.
8. BAHRAMI, Z., PEDRAM-NIA, A., SAEIDI-ASL, M., ARMIN, M. & HEYDARI-MAJD, M. 2023. Bioactive gliadin electrospinning loaded with Zataria multiflora Boiss essential oil: Improves antimicrobial activity and release modeling behavior. *Food Science & Nutrition*, 11, 307–319.
9. CEC. Commission of the European Community, Decision 95/149/EC of 8 March 1995 fixing the total volatile basic nitrogen (TVB-N) limit values for certain categories of fishery products and specifying the analysis methods to be used. 1995. CEC Brussels.
10. CHEN, L., WANG, W., WANG, W. & ZHANG, J. 2023. Effect of anthocyanins on colorimetric indicator film properties. *Coatings*, 13, 1682.
11. Córdoba, L. J. P., & Sobral, P. J. (2017). Physical and antioxidant properties of films based on gelatin, gelatin-chitosan or gelatin-sodium caseinate blends loaded with nanoemulsified active compounds. *Journal of Food Engineering*, *213*, 47–53.
12. Dangles, O., & Fenger, J.-A. (2018). The chemical reactivity of anthocyanins and its consequences in food science and nutrition. *Molecules*, *23*(8), 1970.
13. Flórez, M., Guerra-Rodríguez, E., Cazón, P., & Vázquez, M. (2022). Chitosan for food packaging: Recent advances in active and intelligent films. *Food hydrocolloids*, *124*, 107328.
14. Ghorbani, M., Divsalar, E., Molaei, R., Ezati, P., Moradi, M., Tajik, H., & Abbaszadeh, M. (2021). A halochromic indicator based on polylactic acid and anthocyanins for visual freshness monitoring of minced meat, chicken fillet, shrimp, and fish roe. *Innovative Food Science & Emerging Technologies*, *74*, 102864.
15. Habtemariam, S. (2019). *Medicinal foods as potential therapies for Type-2 diabetes and associated diseases: the chemical and pharmacological basis of their action*. Academic Press.
16. Hanani, Z. N., Yee, F. C., & Nor-Khaizura, M. (2019). Effect of pomegranate (Punica granatum L.) peel powder on the antioxidant and antimicrobial properties of fish gelatin films as active packaging. *Food hydrocolloids*, *89*, 253–259.
17. He, Y., Lu, L., Lin, Y., Li, R., Yuan, Y., Lu, X., Zou, Y., Zhou, W., Wang, Z., & Li, J. (2022). Intelligent pH-sensing film based on polyvinyl alcohol/cellulose nanocrystal with purple cabbage anthocyanins for visually monitoring shrimp freshness. *International Journal of Biological Macromolecules*, *218*, 900–908.
18. HEYDARI-MAJD, M., GHANBARZADEH, B., SHAHIDI-NOGHABI, M., NAJAFI, M. A. & HOSSEINI, M. 2019a. A new active nanocomposite film based on PLA/ZnO nanoparticle/essential oils for the preservation of refrigerated Otolithes ruber fillets. *Food Packaging and Shelf Life*, 19, 94–103.

19. HEYDARI-MAJD, M., REZAEINIA, H., SHADAN, M. R., GHORANI, B. & TUCKER, N. 2019b. Enrichment of zein nanofibre assemblies for therapeutic delivery of Barije (Ferula gummosa Boiss) essential oil. *Journal of Drug Delivery Science and Technology*, 54, 101290.
20. HEYDARI-MAJD, M., SHADAN, M. R., REZAEINIA, H., GHORANI, B., BAMERI, F., SARABANDI, K. & KHOSHABI, F. 2023. Electrospun plant protein-based nanofibers loaded with sakacin as a promising bacteriocin source for active packaging against Listeria monocytogenes in quail breast. *International Journal of Food Microbiology*, 391, 110143.
21. HEYDARI-MAJD, M., SHAFEGHAT, M. & GHOFRAN-MAKSHOUF, F. 2024. Effect of Zein Nanofiber Containing Barije Essential Oil on Increasing the Storage Time of shrimp (Litopenaeus vannamei) at Refrigerated Temperature (4 ± 1° C). *Research and Innovation in Food Science and Technology*, 12, 313–328.
22. HOSEINPOUR, Z., NIAZMAND, R. & HEYDARI-MAJD, M. 2025a. Extraction and characterization of nanocellulose from Cuminum cyminum L. husk by ball-milling-assisted ultrasound. *Carbohydrate Polymer Technologies and Applications*, 100934.
23. HOSEINPOUR, Z., NIAZMAND, R., PARLAK, M. E., HEYDARI-MAJD, M. & SARICAOGLU, F. T. 2025b. Shear-thinning dynamics and viscoelasticity of a novel Eremurus spectabilis glucomannan: Structural insights and implications for food/pharmaceutical applications. *Carbohydrate Polymer Technologies and Applications*, 100910.
24. Huang, J., Chen, M., Zhou, Y., Li, Y., & Hu, Y. (2020). Functional characteristics improvement by structural modification of hydroxypropyl methylcellulose modified polyvinyl alcohol films incorporating roselle anthocyanins for shrimp freshness monitoring. *International Journal of Biological Macromolecules*, *162*, 1250–1261.
25. Huang, S., Xiong, Y., Zou, Y., Dong, Q., Ding, F., Liu, X., & Li, H. (2019). A novel colorimetric indicator based on agar incorporated with Arnebia euchroma root extracts for monitoring fish freshness. *Food hydrocolloids*, *90*, 198–205.
26. Kang, S., Wang, H., Xia, L., Chen, M., Li, L., Cheng, J., Li, X., & Jiang, S. (2020). Colorimetric film based on polyvinyl alcohol/okra mucilage polysaccharide incorporated with rose anthocyanins for shrimp freshness monitoring. *Carbohydrate Polymers*, *229*, 115402.
27. Karami, N., Lindblom, A., Yazdanshenas, S., Lindén, V., & Åhrén, C. (2020). Recurrence of urinary tract infections with extended-spectrum β-lactamase-producing Escherichia coli caused by homologous strains among which clone ST131-O25b is dominant. *Journal of global antimicrobial resistance*, *22*, 126–132.
28. Karbownik, I., Rac-Rumijowska, O., Fiedot-Toboła, M., Rybicki, T., & Teterycz, H. (2019). The preparation and characterization of polyacrylonitrile-polyaniline (PAN/PANI) fibers. *Materials*, *12*(4), 664.
29. Kurek, M., Garofulić, I. E., Bakić, M. T., Ščetar, M., & Uzelac, V. D. (2018). Development and evaluation of a novel antioxidant and pH indicator film based on chitosan and food waste sources of antioxidants. *Food hydrocolloids*, *84*, 238–246.

30. KYRANA, V. R. & LOUGOVOIS, V. P. 2002. Sensory, chemical and microbiological assessment of farm-raised European sea bass (Dicentrarchus labrax) stored in melting ice. *International Journal of Food Science and Technology*, 37, 319–328.
31. KYRANA, V. R., LOUGOVOIS, V. P. & VALSAMIS, D. S. 1997. Assessment of shelf-life of maricultured gilthead sea bream (Sparus aurata) stored in ice. *International Journal of Food Science and Technology*, 32, 339–347.
32. Li, H., Wei, J., Jin, M., Yu, Y., Bu, J., Chen, Q., & Hao, Z. (2022). Colorimetric analysis through electrospun WO3/PAN membrane for indication of oxygen in food packaging using a smartphone. *Composites Communications*, *35*, 101321.
33. Liu, Y., Qin, Y., Bai, R., Zhang, X., Yuan, L., & Liu, J. (2019). Preparation of pH-sensitive and antioxidant packaging films based on κ-carrageenan and mulberry polyphenolic extract. *International Journal of Biological Macromolecules*, *134*, 993–1001.
34. Lu, W., Chen, M., Cheng, M., Yan, X., Zhang, R., Kong, R., Wang, J., & Wang, X. (2021). Development of antioxidant and antimicrobial bioactive films based on Oregano essential oil/mesoporous nano-silica/sodium alginate. *Food Packaging and Shelf Life*, *29*, 100691.
35. Luo, X., Zaitoon, A., & Lim, L. T. (2022). A review on colorimetric indicators for monitoring product freshness in intelligent food packaging: Indicator dyes, preparation methods, and applications. *Comprehensive reviews in food science and food safety*, *21*(3), 2489–2519.
36. MEMDUEVA, N., TZANOVA, M., YANEVA, Z., RUSENOVA, N., GROZEVA, N. & DINEV, T. 2025. Natural Deep Eutectic Solvent-Based Extraction of Malva sylvestris L.: Phytochemical Content, Antioxidant and Antimicrobial Potential. *Separations*, 12, 187.
37. Min, T., Zhou, L., Sun, X., Du, H., Zhu, Z., & Wen, Y. (2022). Electrospun functional polymeric nanofibers for active food packaging: A review. *Food Chemistry*, *391*, 133239.
38. Moradi, M., Tajik, H., Almasi, H., Forough, M., & Ezati, P. (2019). A novel pH-sensing indicator based on bacterial cellulose nanofibers and black carrot anthocyanins for monitoring fish freshness. *Carbohydrate Polymers*, *222*, 115030.
39. Mushtaq, M., Gani, A., Gani, A., Punoo, H. A., & Masoodi, F. (2018). Use of pomegranate peel extract incorporated zein film with improved properties for prolonged shelf life of fresh Himalayan cheese (Kalari/kradi). *Innovative Food Science & Emerging Technologies*, *48*, 25–32.
40. MUSHTAQ, M., JINDANI, R., FAROOQ, A., LI, X., SABA, H., WASIM, M., WEI, Q. & SIDDIQUI, Q. 2022. Characterization of electrospun polylactide nanofibers modified via atom transfer radical polymerization. *Journal of Industrial Textiles*, 51, 1175S-1185S.
41. NIAZMAND, R., SHARAYEI, P., HEYDARI-MAJD, M. & SAYAHI, M. 2025. Optimization of a novel antimicrobial nanocomposite films based on starch saffron corm incorporating nanoclay/lignin/extract using response surface methodology. *International Journal of Biological Macromolecules*, 307, 141733.
42. NOGHANI BAHAMBARI, F., RAJABI ISLAMI, H. & SHAMSAIE MEHRGAN, M. 2024. Extract of common mallow (Malva sylvestris) petals incorporated in starch/tragacanth gum film as a

halochromic indicator for monitoring of Nile tilapia (Oreochromis niloticus) fillet quality. *Journal of Food Measurement and Characterization*, 18, 4161–4176.

43. Nunes, J. C., Melo, P. T. S., Lorevice, M. V., Aouada, F. A., & de Moura, M. R. (2021). Effect of green tea extract on gelatin-based films incorporated with lemon essential oil. *Journal of food science and technology*, *58*(1), 1–8.
44. PACQUIT, A., LAU, K. T., MCLAUGHLIN, H., FRISBY, J., QUILTY, B. & DIAMOND, D. 2006. Development of a volatile amine sensor for the monitoring of fish spoilage. *Talanta*, 69, 515–520.
45. Prietto, L., Pinto, V. Z., El Halal, S. L. M., de Morais, M. G., Costa, J. A. V., Lim, L. T., Dias, A. R. G., & Zavareze, E. d. R. (2018). Ultrafine fibers of zein and anthocyanins as natural pH indicator. *Journal of the Science of Food and Agriculture*, *98*(7), 2735–2741.
46. Qin, Y., Liu, Y., Zhang, X., & Liu, J. (2020). Development of active and intelligent packaging by incorporating betalains from red pitaya (Hylocereus polyrhizus) peel into starch/polyvinyl alcohol films. *Food hydrocolloids*, *100*, 105410.
47. Safaee-Ardakani, M. R., Hatamian-Zarmi, A., Sadat, S. M., Mokhtari-Hosseini, Z. B., Ebrahimi-Hosseinzadeh, B., Kooshki, H., & Rashidiani, J. (2019). In situ preparation of PVA/schizophyllan-AgNPs nanofiber as potential of wound healing: characterization and cytotoxicity. *Fibers and Polymers*, *20*, 2493–2502.
48. Seddighfar, M., Mirghazanfari, S. M., & Dadpay, M. (2020). Analgesic and anti-inflammatory properties of hydroalcoholic extracts of Malva sylvestris, Carum carvi or Medicago sativa, and their combination in a rat model. *Journal of integrative medicine*, *18*(2), 181–188.
49. Shakouri, M., Salami, M., Lim, L.-T., Ekrami, M., Mohammadian, M., Askari, G., Emam-Djomeh, Z., & McClements, D. J. (2023). Development of active and intelligent colorimetric biopolymer indicator: Anthocyanin-loaded gelatin-basil seed gum films. *Journal of Food Measurement and Characterization*, *17*(1), 472–484.
50. Shavisi, N., & Shahbazi, Y. (2022). Chitosan-gum Arabic nanofiber mats encapsulated with pH-sensitive Rosa damascena anthocyanins for freshness monitoring of chicken fillets. *Food Packaging and Shelf Life*, *32*, 100827.
51. Shivangi, S., Dorairaj, D., Negi, P. S., & Shetty, N. P. (2021). Development and characterisation of a pectin-based edible film that contains mulberry leaf extract and its bio-active components. *Food hydrocolloids*, *121*, 107046.
52. SILVA-PEREIRA, M. C., TEIXEIRA, J. A., PEREIRA-JÚNIOR, V. A. & STEFANI, R. 2015. Chitosan/corn starch blend films with extract from Brassica oleraceae (red cabbage) as a visual indicator of fish deterioration. *LWT-Food Science and Technology*, 61, 258–262.
53. Sun, J., Du, Y., Ma, J., Li, Y., Wang, L., Lu, Y., Zou, J., Pang, J., & Wu, C. (2019). Transparent bionanocomposite films based on konjac glucomannan, chitosan, and TEMPO-oxidized chitin nanocrystals with enhanced mechanical and barrier properties. *International Journal of Biological Macromolecules*, *138*, 866–873.

54. Tretsiakova-McNally, S., & Joseph, P. (2018). Thermal and calorimetric evaluations of polyacrylonitrile containing covalently-bound phosphonate groups. *Polymers*, *10*(2), 131.
55. Turalija, M., Bischof, S., Budimir, A., & Gaan, S. (2016). Antimicrobial PLA films from environment friendly additives. *Composites Part B: Engineering*, *102*, 94–99.
56. VARELA, P., ÁLVAREZ-CARRASCO, F., SARABIA-VALLEJOS, M., GARCÍA-HERRERA, C., ZAPATA, P. A., PEPONI, L., MARTINEZ, J. J., ZÁRATE, D. & CANALES, D. A. 2025. Electrospun Polyacrylonitrile-Based Scaffolds Reinforced with Argopecten purpuratus-Derived CaO for Enhanced Biomedical Functionality. *ACS Applied Polymer Materials*, 7, 12269–12282.
57. WARIS, T. S., AKHTAR, A. & YAR, M. 2025. Electrospun scaffolds for soft tissue (muscle, fibrous tissue, blood vessels, and supporting tissue) applications. *Electrospun Biomaterials for Tissue Engineering and Drug Delivery Applications*. Elsevier.
58. Wang, Y. X., Wang, C. G., Wu, J. W., & Jing, M. (2007). High-temperature DSC study of polyacrylonitrile precursors during their conversion to carbon fibers. *Journal of Applied Polymer Science*, *106*(3), 1787–1792.
59. Yavari Maroufi, L., PourvatanDoust, S., Naeijian, F., & Ghorbani, M. (2022). Fabrication of electrospun polycaprolactone/casein nanofibers containing green tea essential oils: Applicable for active food packaging. *Food and Bioprocess Technology*, *15*(11), 2601–2615.
60. Yong, H., Wang, X., Bai, R., Miao, Z., Zhang, X., & Liu, J. (2019). Development of antioxidant and intelligent pH-sensing packaging films by incorporating purple-fleshed sweet potato extract into chitosan matrix. *Food hydrocolloids*, *90*, 216–224.
61. Zhai, X., Shi, J., Zou, X., Wang, S., Jiang, C., Zhang, J., Huang, X., Zhang, W., & Holmes, M. (2017). Novel colorimetric films based on starch/polyvinyl alcohol incorporated with roselle anthocyanins for fish freshness monitoring. *Food hydrocolloids*, *69*, 308–317.
62. Zhang, L., Liu, Z., Han, X., Sun, Y., & Wang, X. (2019). Effect of ethanol content on rheology of film-forming solutions and properties of zein/chitosan film. *International Journal of Biological Macromolecules*, *134*, 807–814.
63. ZHANG, W., HUANG, C., KUSMARTSEVA, O., THOMAS, N. L. & MELE, E. 2017. Electrospinning of polylactic acid fibres containing tea tree and manuka oil. *Reactive and Functional Polymers*, 117, 106–111.
64. Zhang, Z., Wu, Y., Wang, Z., Zou, X., Zhao, Y., & Sun, L. (2016). Fabrication of silver nanoparticles embedded into polyvinyl alcohol (Ag/PVA) composite nanofibrous films through electrospinning for antibacterial and surface-enhanced Raman scattering (SERS) activities. *Materials Science and Engineering: C*, *69*, 462–469.

Figures

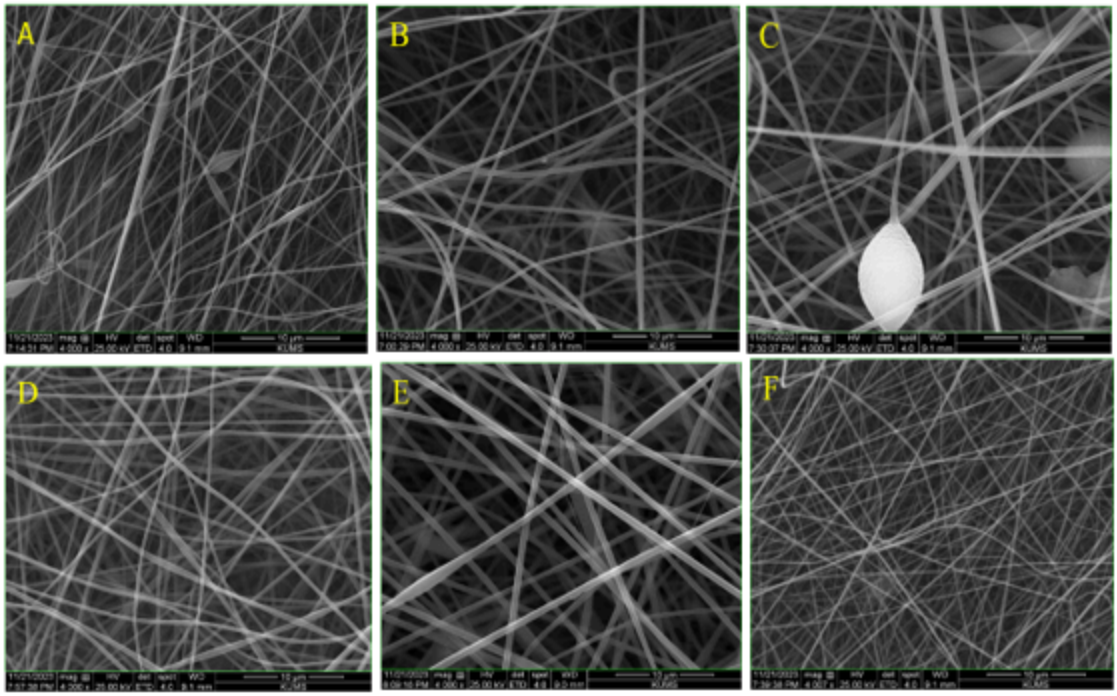


Figure 1

The SEM images of A) PAN 10%, B) PAN 13%, C) PAN 16%, D) PAN/MFE I, E) PAN/MFE II, F) PAN/MFE III

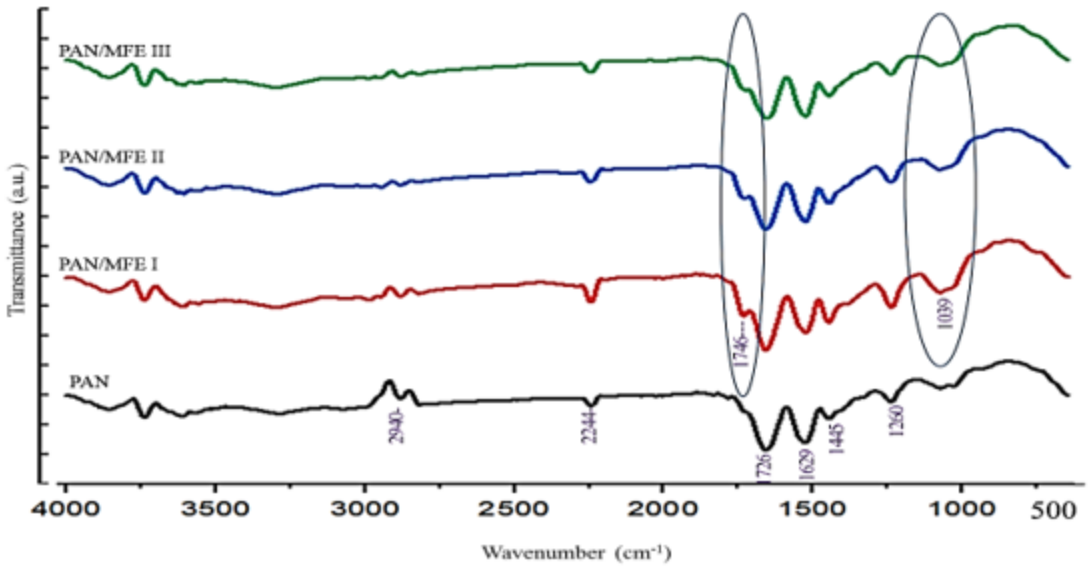


Figure 2

FTIR spectra of PAN, PAN/MFE I, PAN/MFE II, and PAN/MFE III indicator.

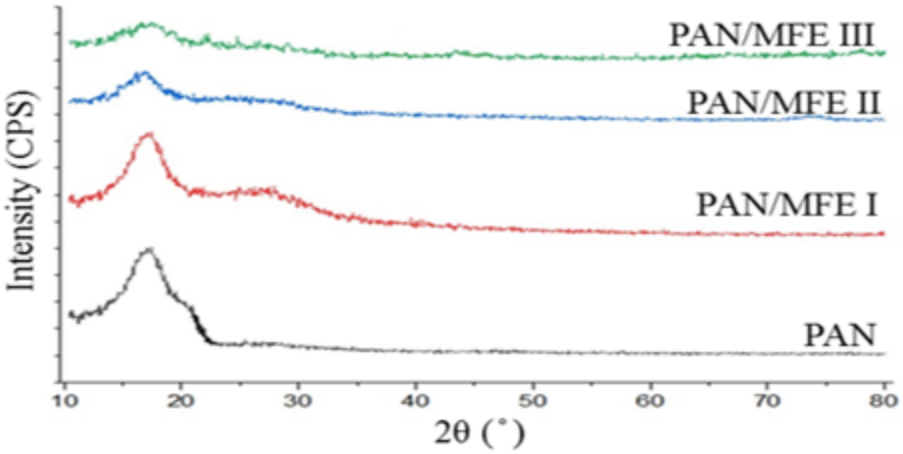


Figure 3

XRD patterns PAN and PAN/MFE nanofibers.

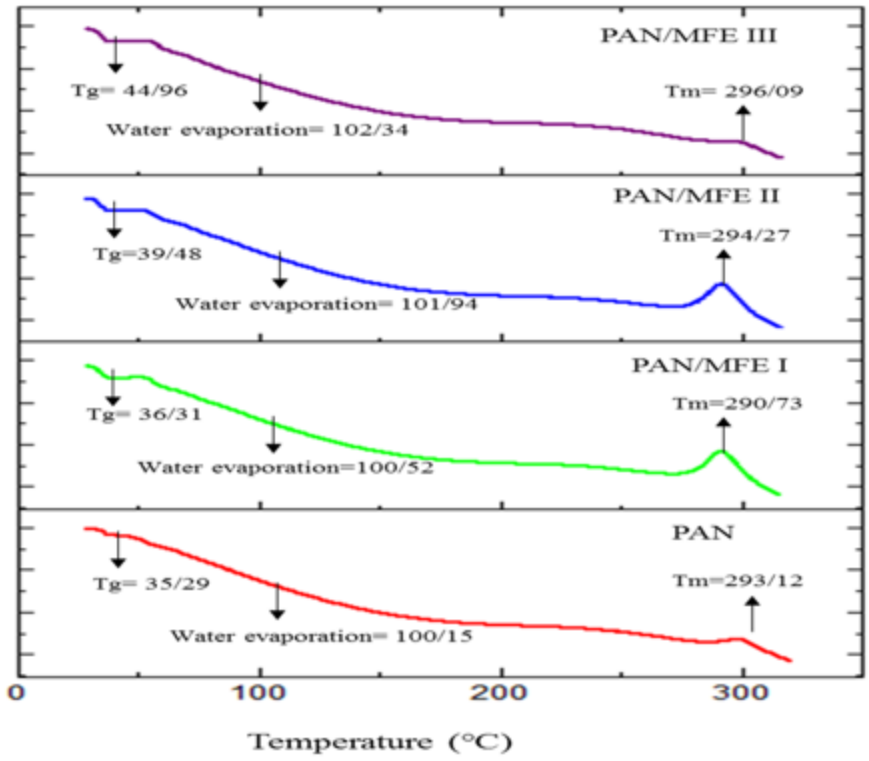


Figure 4

DSC curves of PAN/MFE nanofibers.

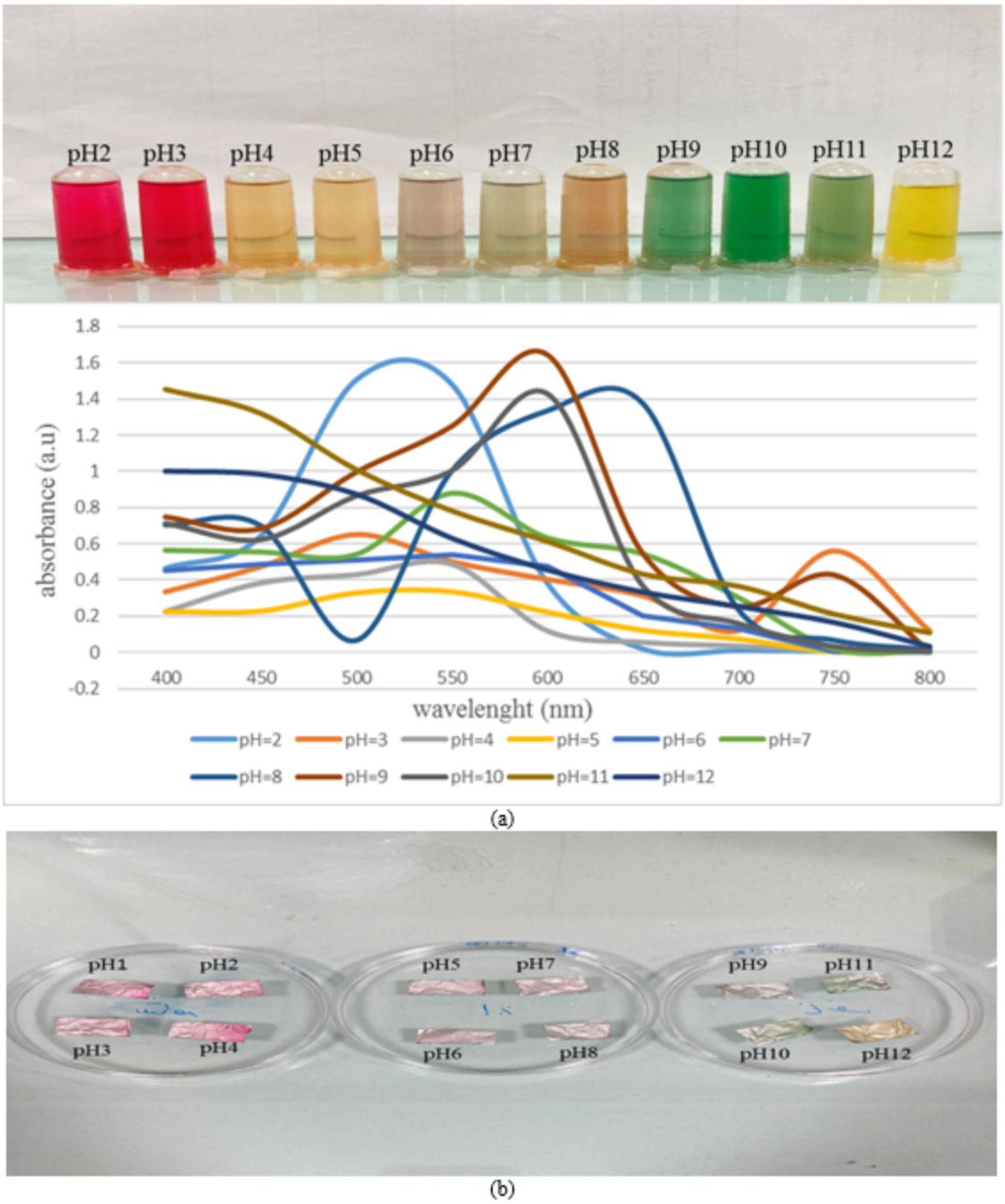


Figure 5

Color variations and UV–vis spectra of MFE (a) and PAN/MFE indicator (b) at various pH values.

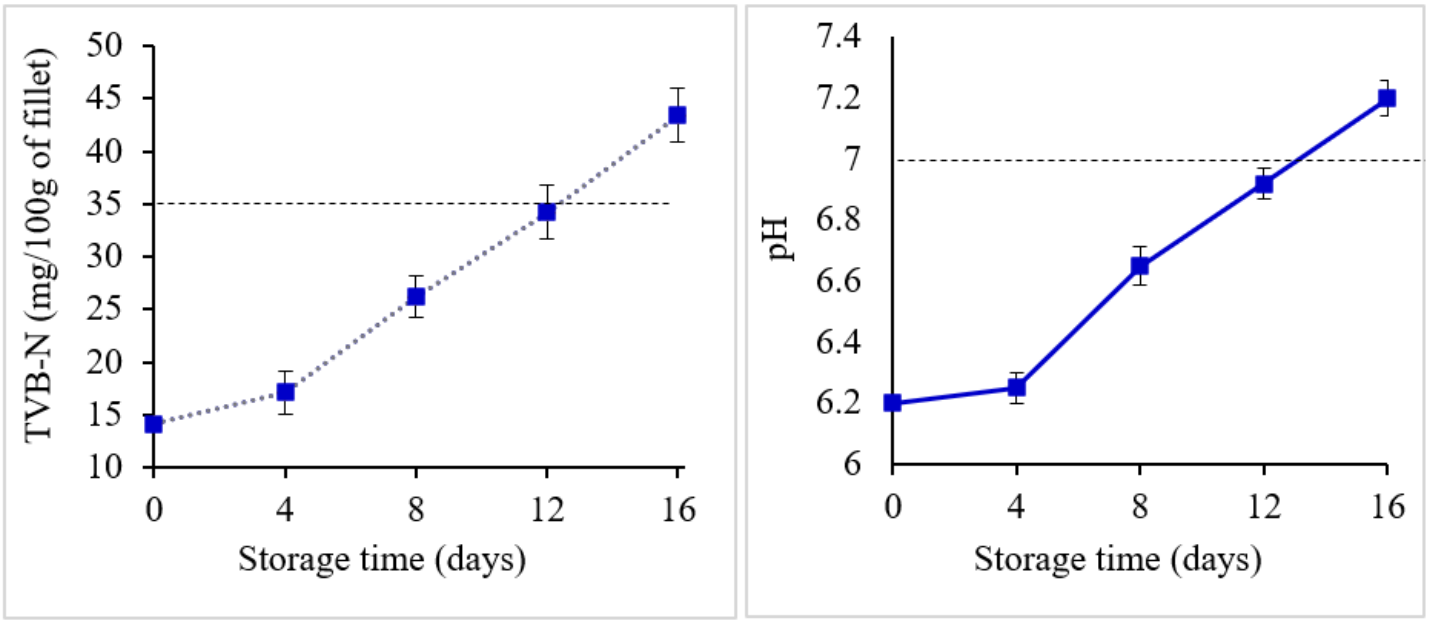


Figure 6

Changes in (a), TVB-N and (b), pH values of *O. ruber*fillets during storage in refrigerator. Data are shown as mean ± SD of three independent measurements.

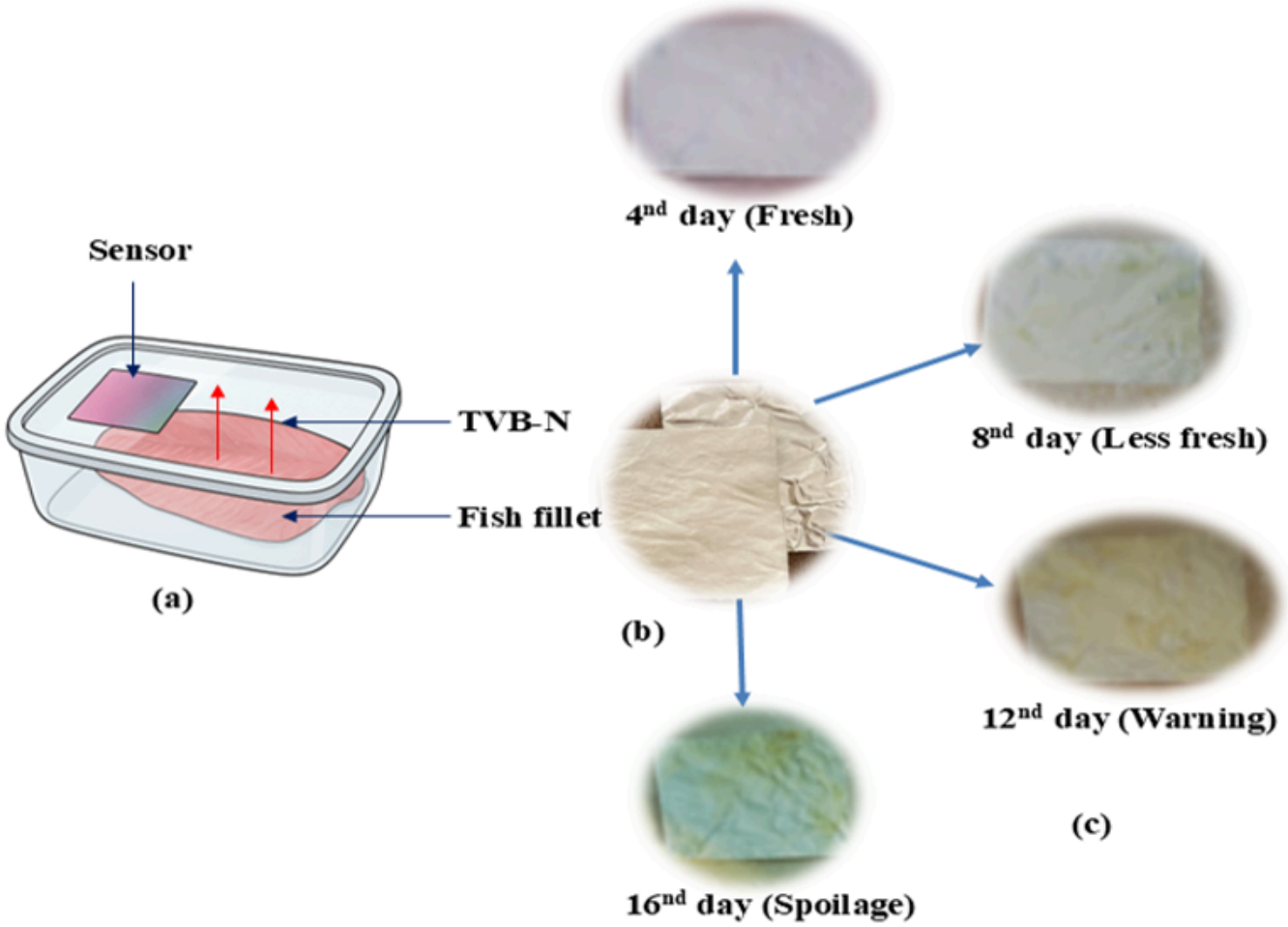


Figure 7

Schematic illustration of the non-contact PAN/MFE nanosensor attached to the inner lid of a polypropylene container (a), electrospun PAN nanofibers incorporating MFE (b), and the color evolution of the halochromic nanosensor over storage time (4, 8, 12, and 16 days) (c).